Supplementary Information

Enhanced Tin Halide Perovskite Solar Cells via Crystal Growth Control Using a Multifunctional Interfacial Modifier

*Jun Ryu [1], Padmini Pandey [2], Saemon Yoon [1], Sung-Won Cho [1], Seojun Lee [1], Rashi Kedia [2], Jincheol Kim [3], Jongsung Park [4, *] and Dong-Won Kang [1, 2, *]*

[1] Department of Smart Cities, Chung-Ang University, 84 Heukseok-ro, Dongjak-gu, Seoul 069 74, Republic of Korea.

[2] Department of Energy Systems Engineering, Chung-Ang University, 84 Heukseok-ro, Dongja k-gu, Seoul 06974, Republic of Korea.

[3] School of Engineering, Macquarie University, Sydney, NSW 2109, Australia

[4] Department of Energy Engineering, Department of Energy System Engineering, Gyeongsang National University, Jinju, Gyeongnam 52828, Republic of Korea

* Corresponding author: D-. W. Kang (E-mail: kangdwn@cau.ac.kr), J. Park (E-mail: j.park@gnu.ac.kr)

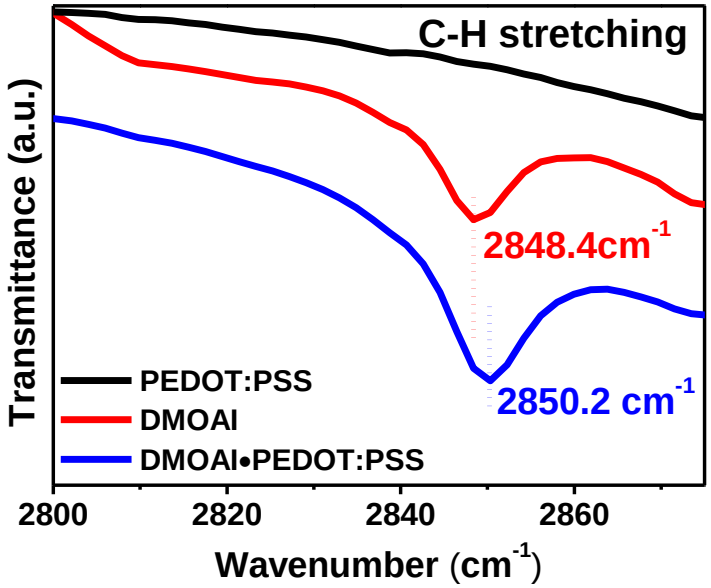

Figure S1. Liquid state FT-IR spectroscopy comparative analysis of the PEDOT: PSS, DMOAI, and DMOAI•PEDOT:PSS complex of C-H stretching mode.

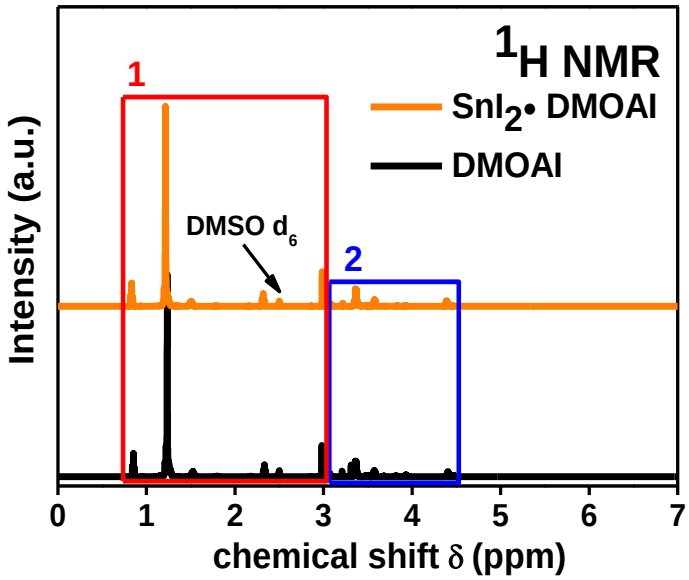

Figure S2. Liquid state ^{1}H NMR full spectra of DMOAI and SnI_2•DMOAI complex in DMSO-d_6.

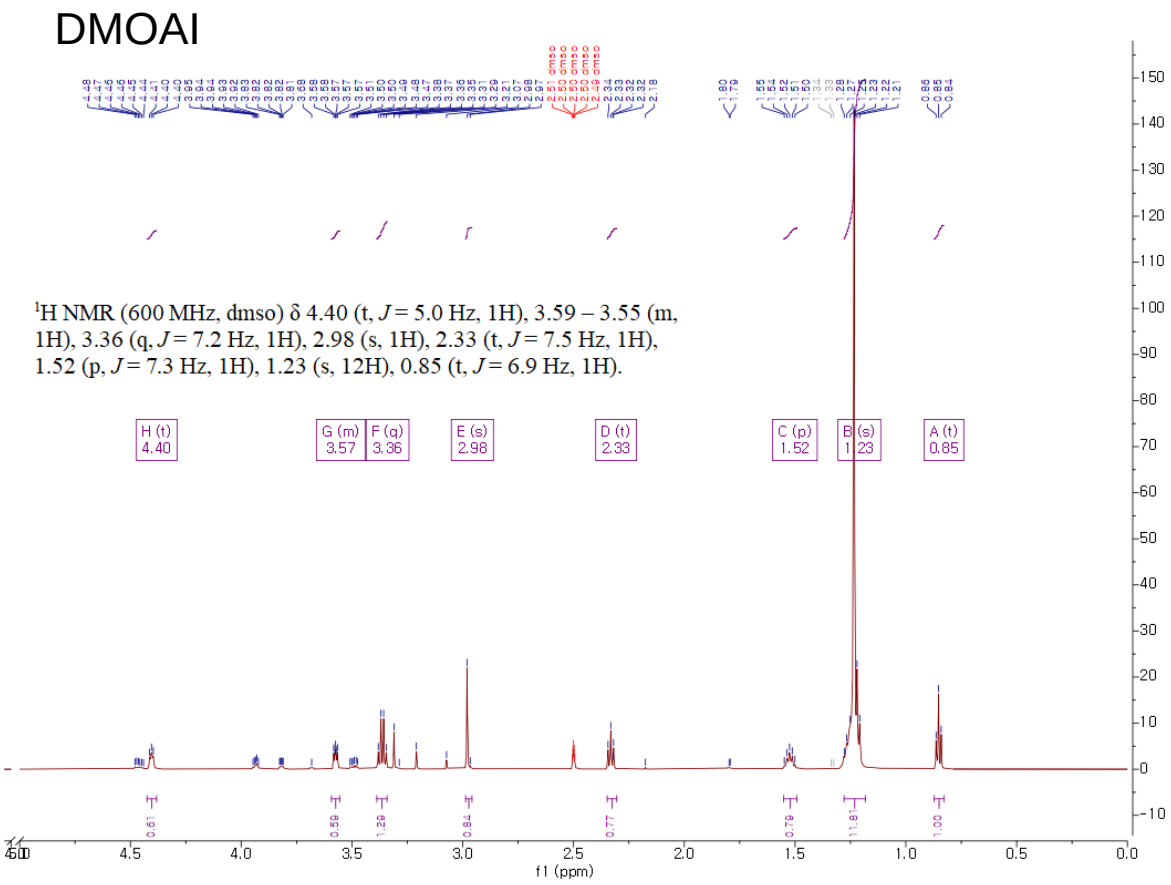

Figure S3. Experimental result of ^{1}H NMR spectrum of DMOAI with estimated chemical shifts.

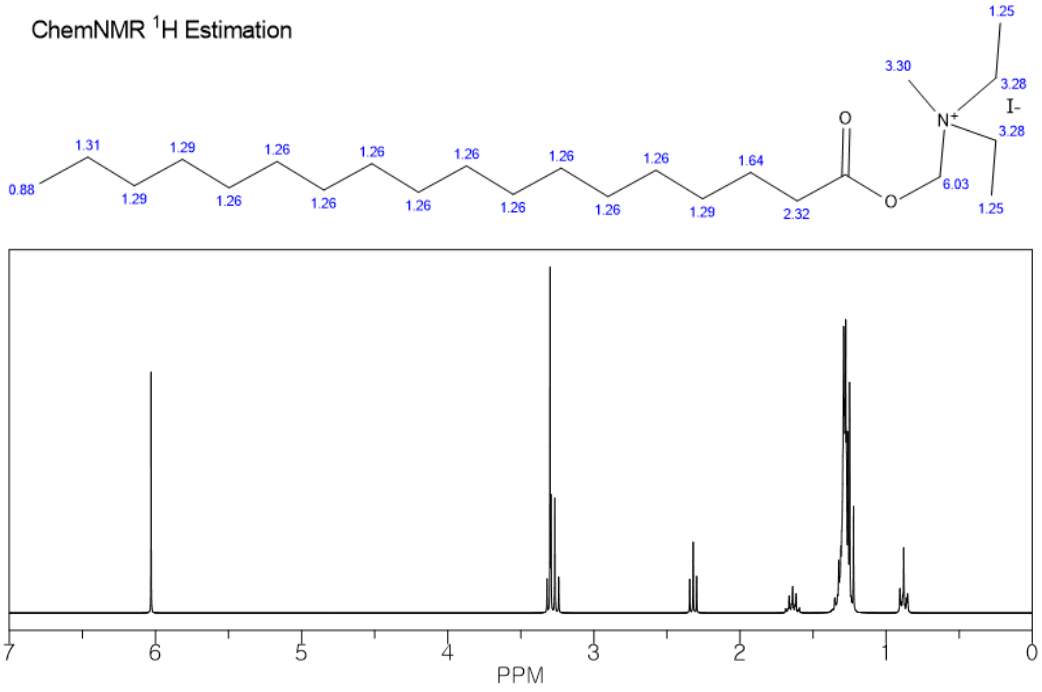

Figure S4. Simulated ^{1}H NMR spectrum of DMOAI, including its molecular structure and estimated chemical shifts.

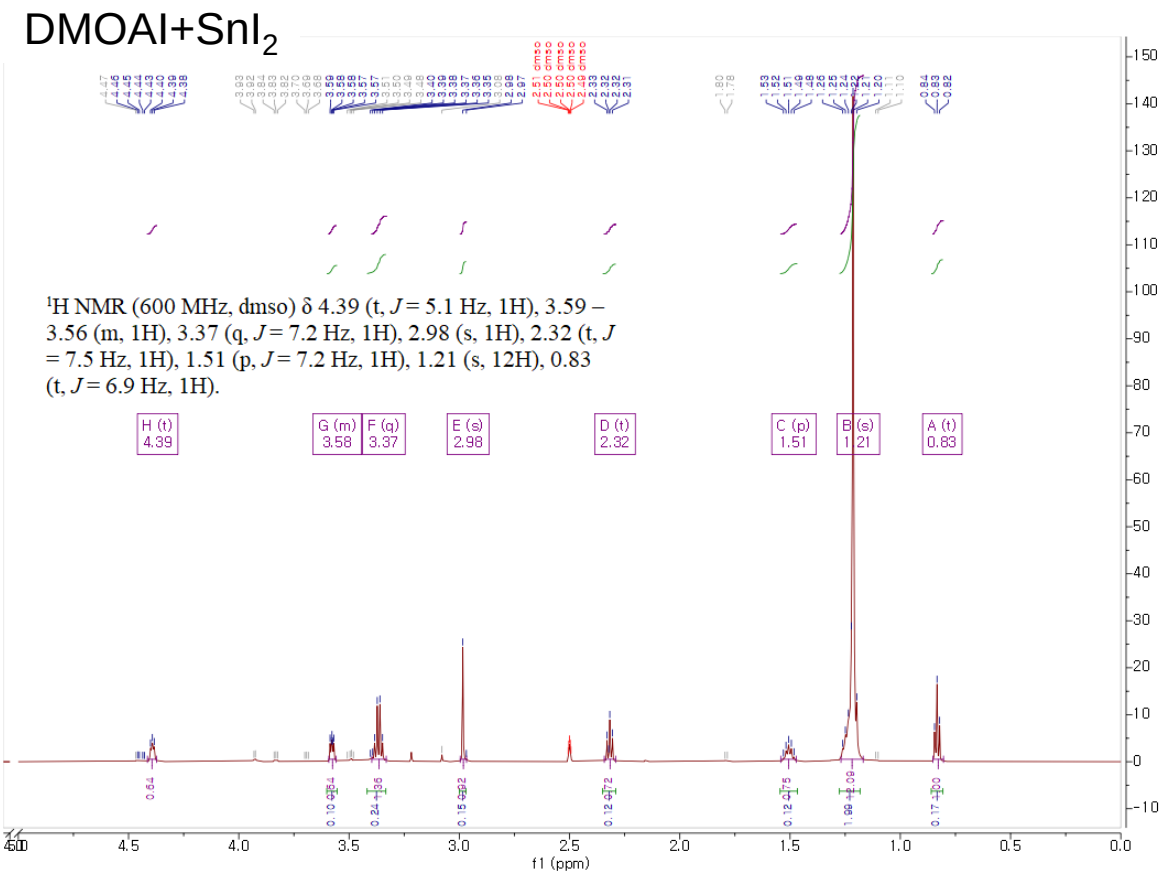

Figure S5. Experimental result of ^{1}H NMR spectrum of SnI_2•DMOAI complex with estimated chemical shifts.

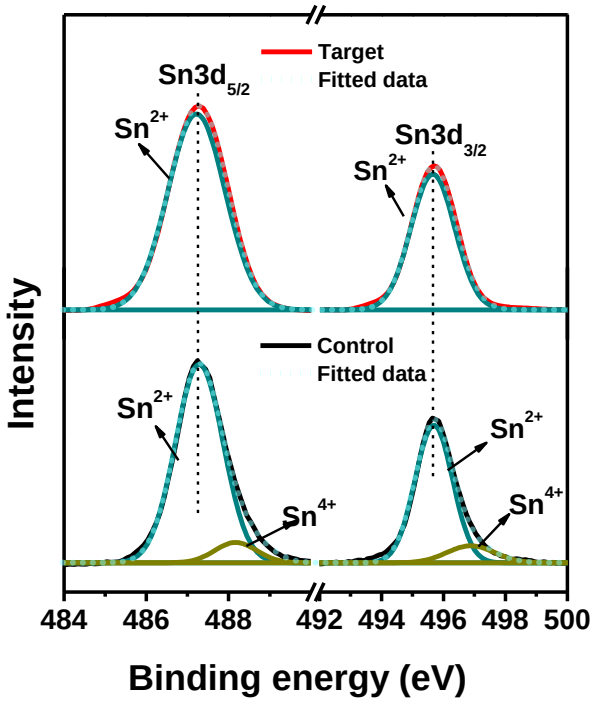

Figure S6. XPS core spectra (a) Sn of control and target Sn-HP films.

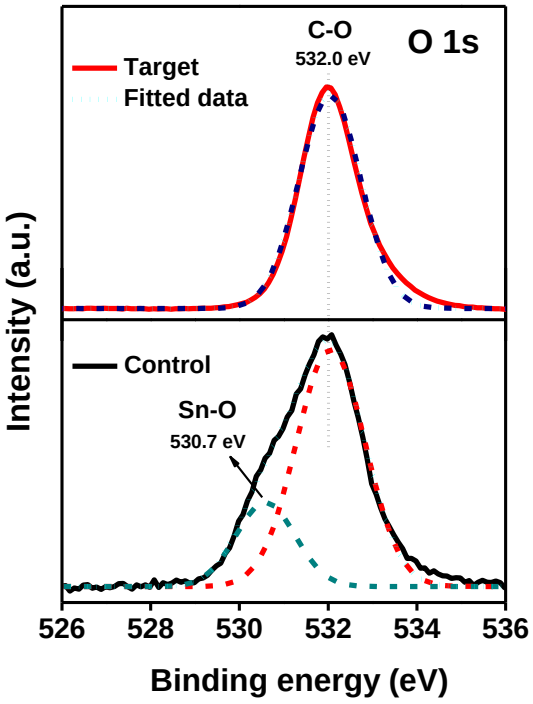

Figure S7. XPS core spectra (a) Sn of control and target Sn-HP films.

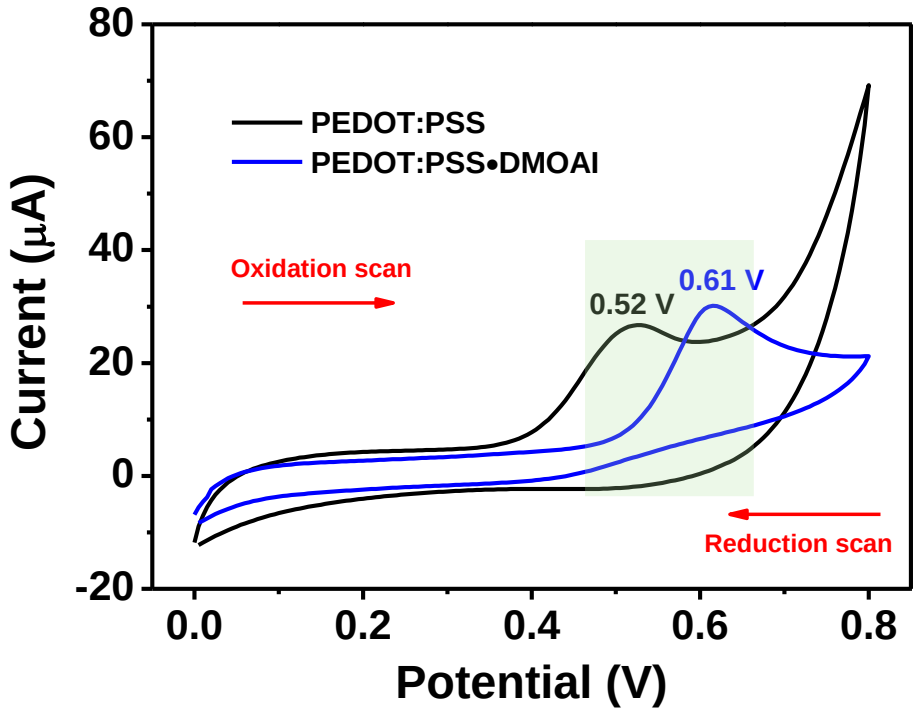

Figure S8. Cyclic voltammetry measurement of PEDOT:PSS and PEDOT:PSS•DMOAI complex films.

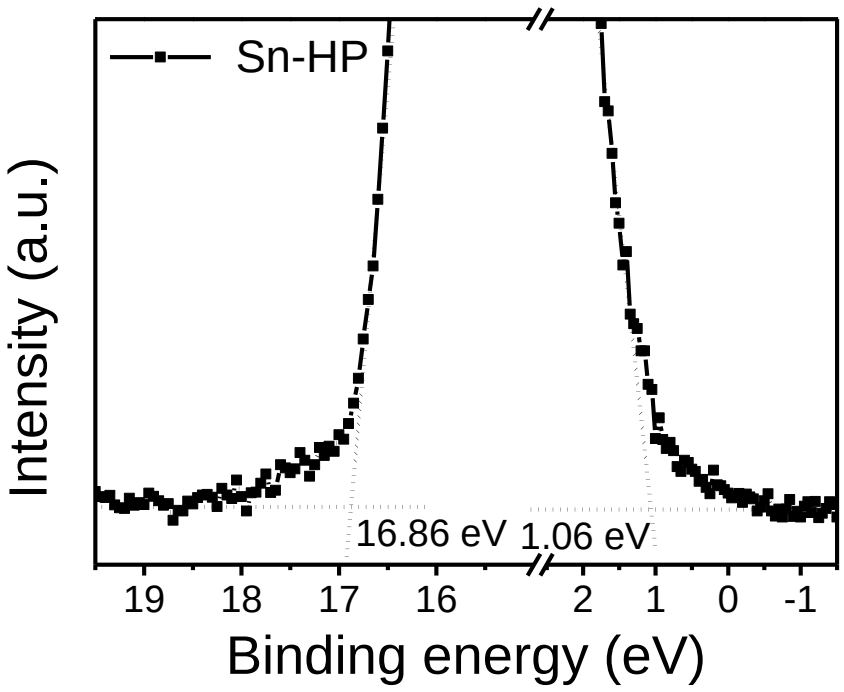

Figure S9. UPS spectrum of Sn-HP.

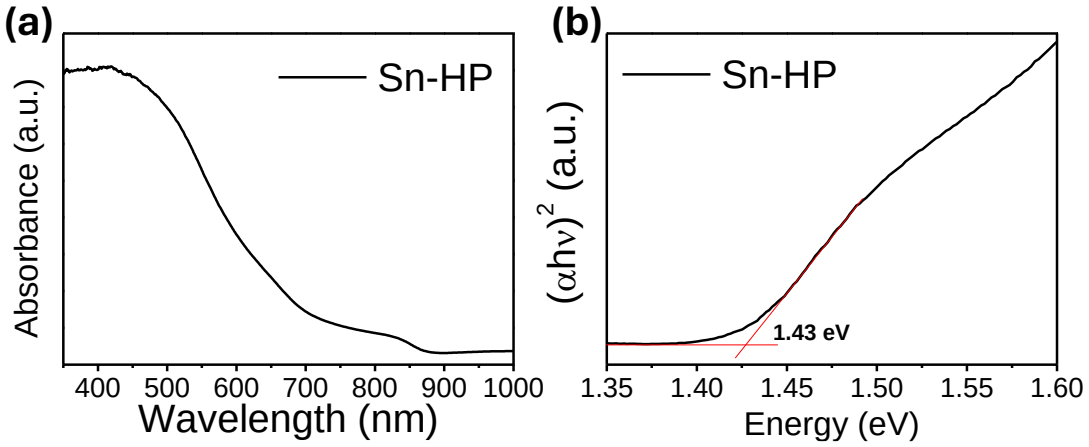

Figure S10. (a) UV-vis absorption spectrum of the Sn-HP film (b) Tauc plot derived from the absorption spectrum.

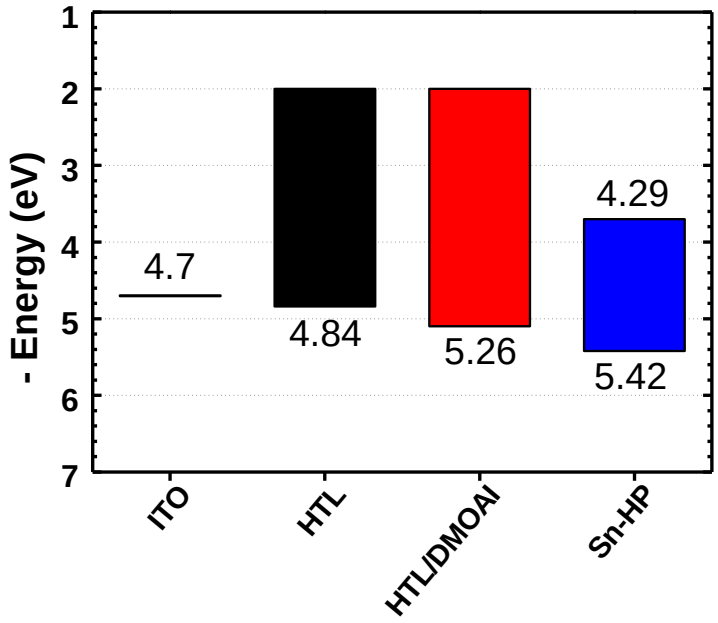

Figure S11. Schematic energy band diagram comparing valence band maximum (VBM) of HTL (PEDOT:PSS) or HTL/DMOAI with Sn-HP layer.

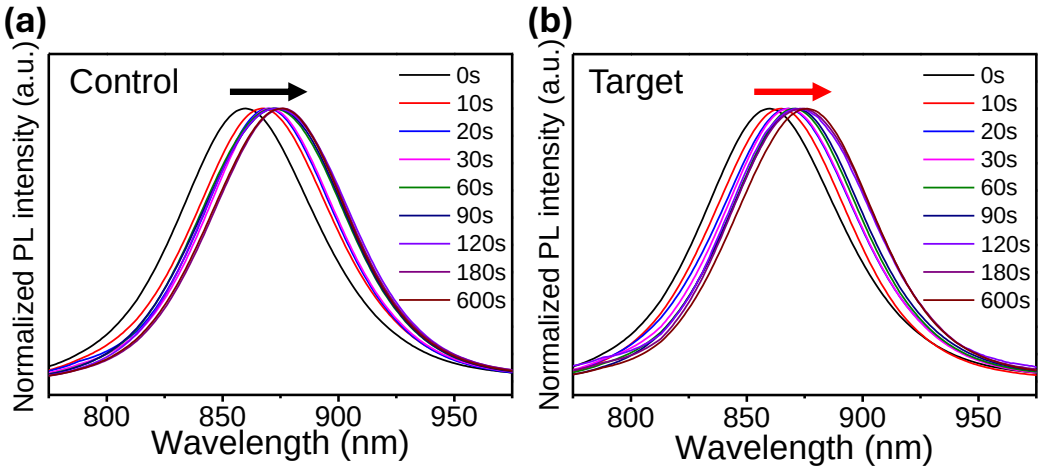

Figure S12. SS-PL dependent on annealing time for Sn-HP growth on (a) PEDOT:PSS (control) and (b) PEDOT:PSS/DMOAI bilayer (target).

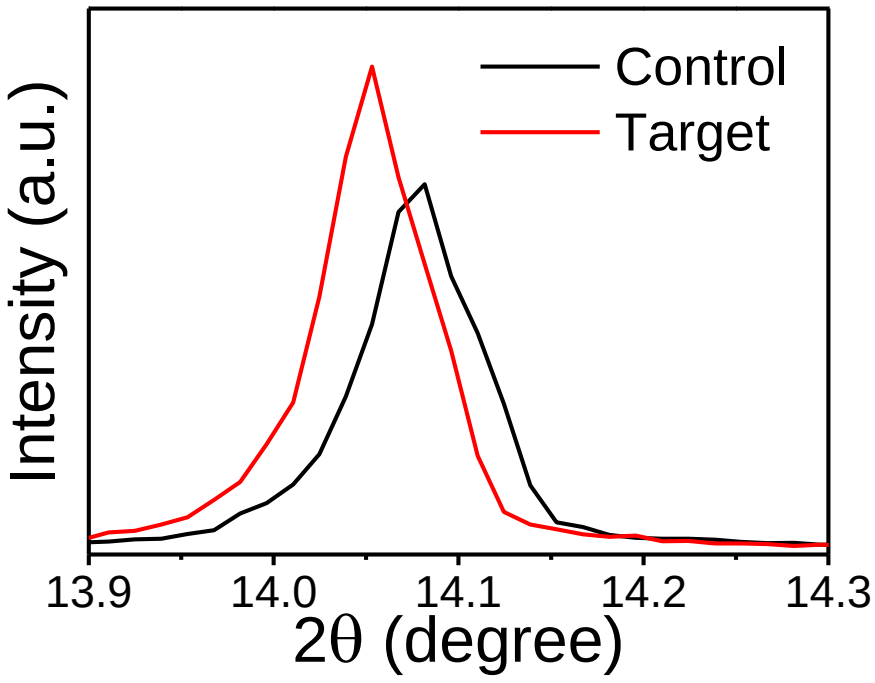

Figure S13. Enlarged XRD pattern corresponding to the (100) plane peak for control and target films.

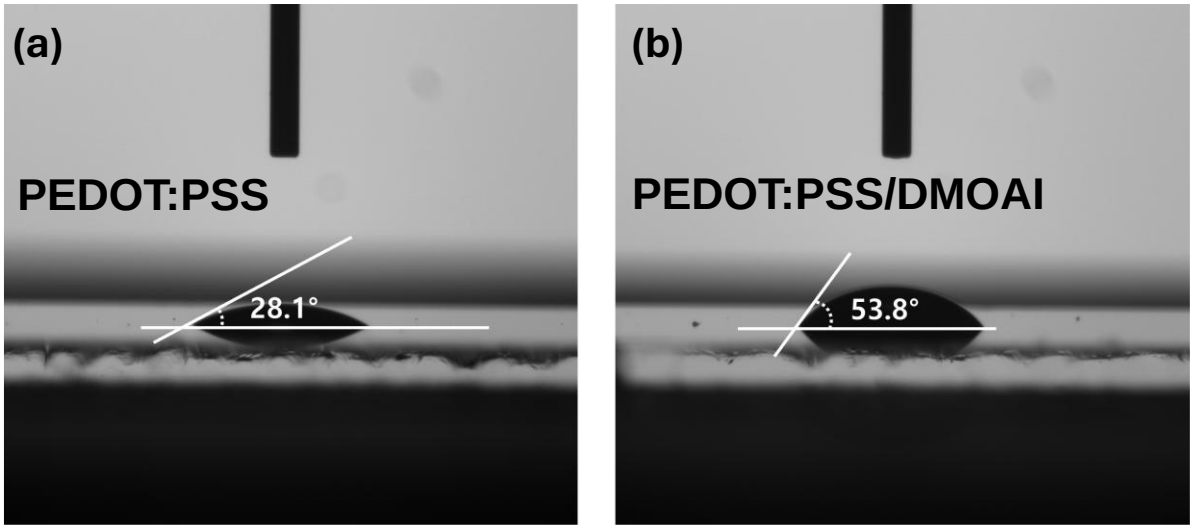

Figure S14. Contact angle of (a) PEDOT:PSS and (b) PEDOT:PSS/DMOAI films using diiodomethane as the solvent.

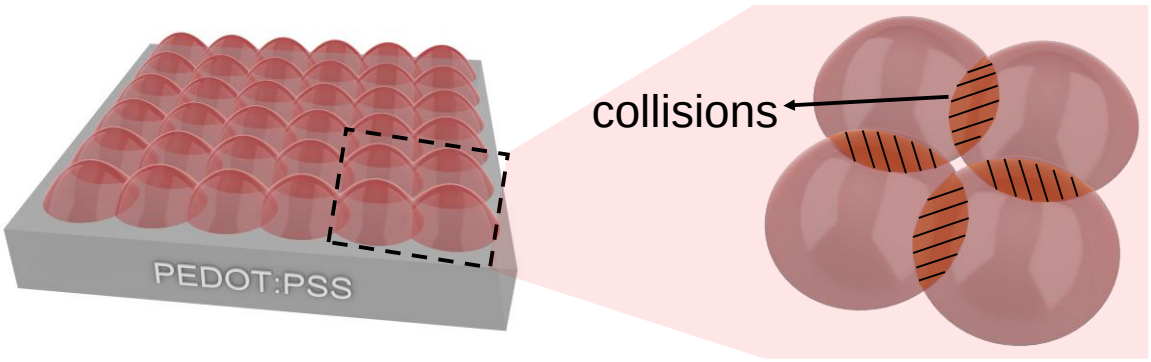

Figure S15. Schematic illustration of crystal collisions during nucleation, induced by an increased density of nuclei.

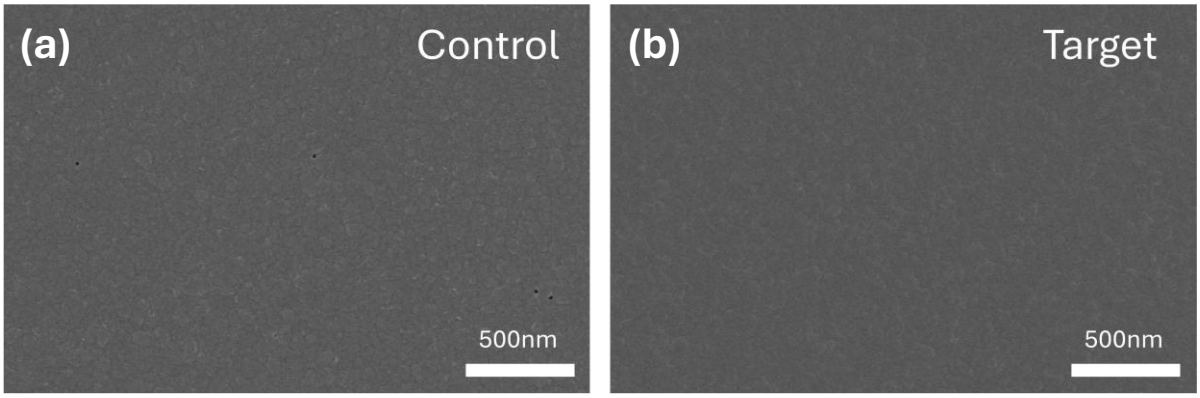

Figure S16. Low-magnification FE-SEM top view image of (a) Control and (b) Target.

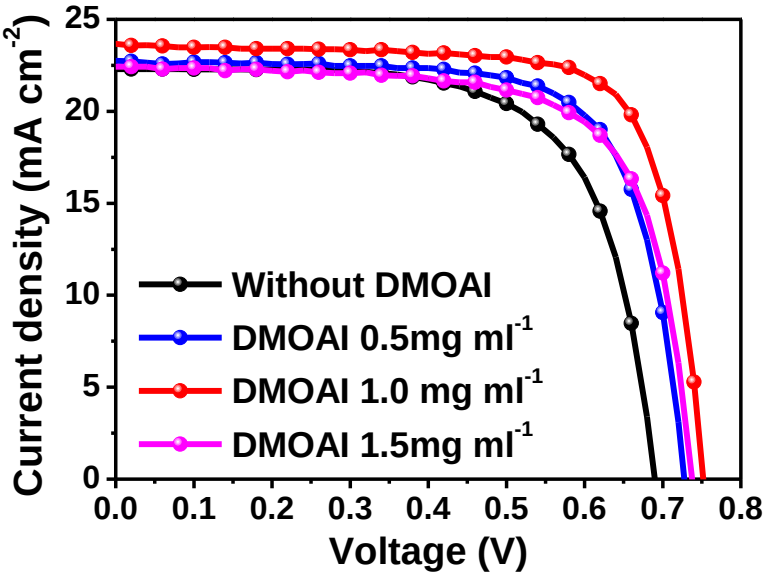

Figure S17. J-V characteristic curves for various concentrations of DMOAI based Sn-HPSCs.

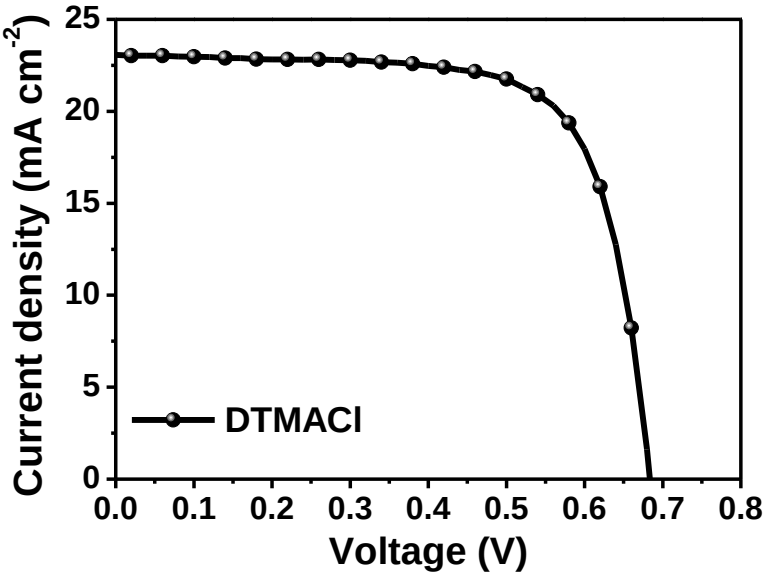

Figure S18. J-V characteristic curves of DTMACl based Sn-HPSC.

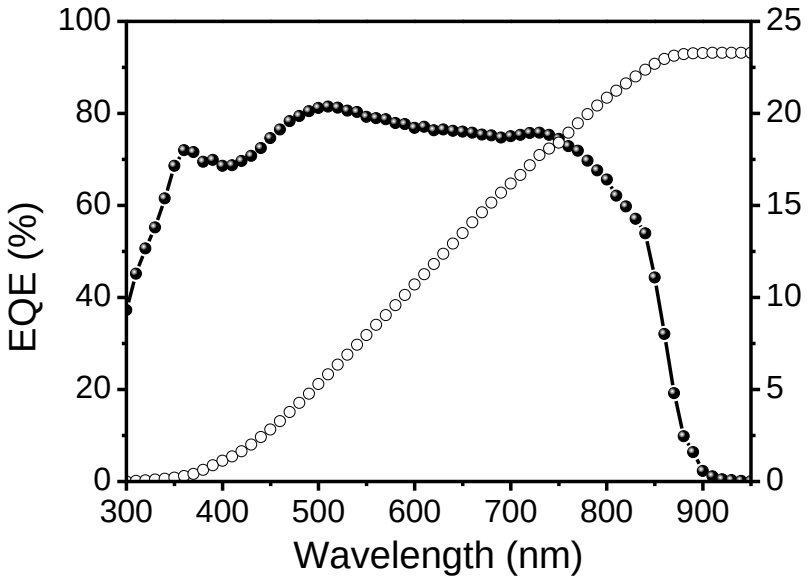

Figure S19. EQE and integrated J_{SC} of DTMACl based Sn-HPSC.

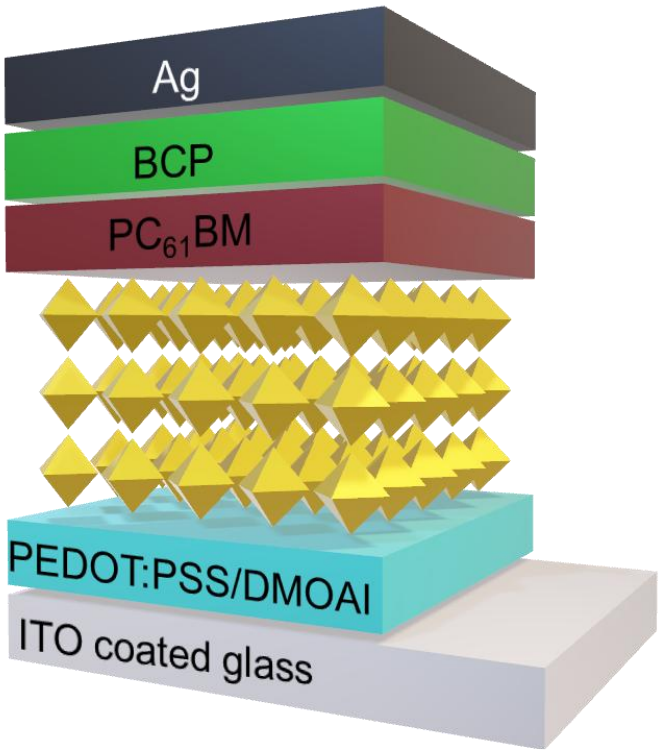

Figure S20. Schematic illustration of wide-bandgap Sn-HPSC structure.

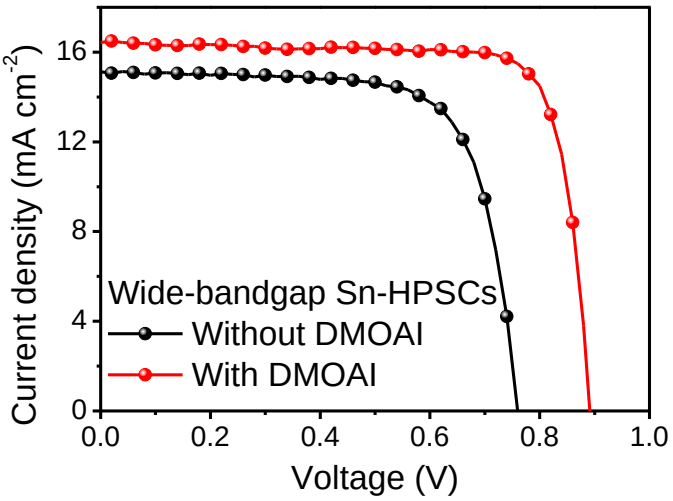

Figure S21. J-V characteristic curves for wide-bandgap Sn-HPSCs without and with DMOAI.

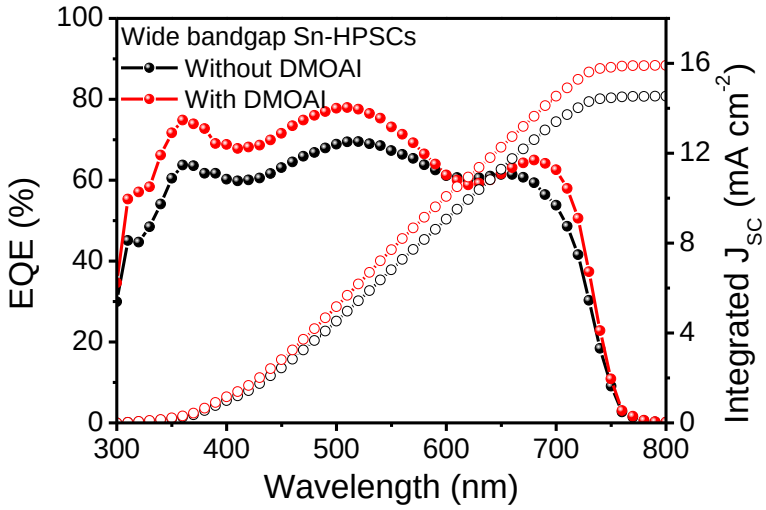

Figure S22. EQE and integrated J_{SC} of wide-bandgap Sn-HPSCs without and with DMOAI.

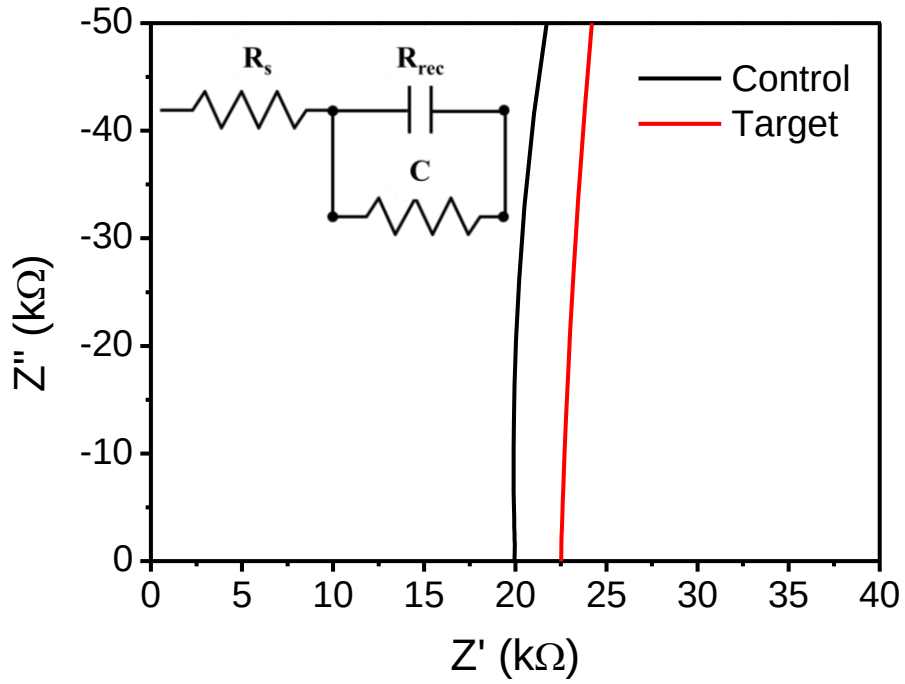

Figure S23. Nyquist plots for control and target devices, with an equivalent circuit diagram representation in the high-frequency region.

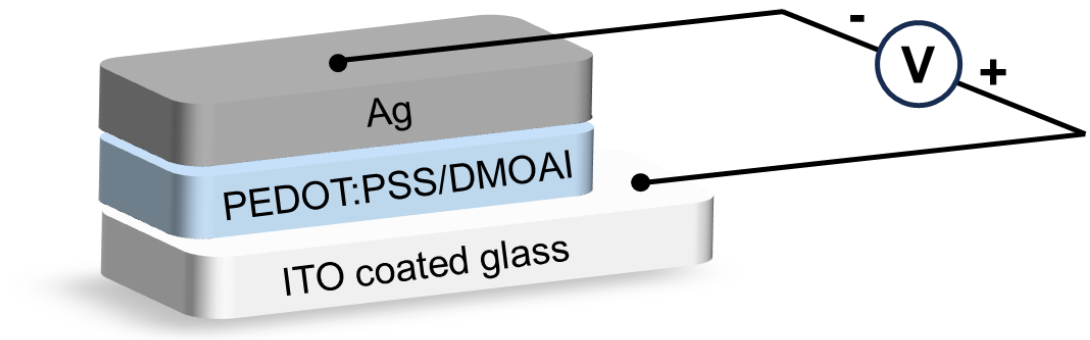

Figure S24. Illustration of the device structure for HTL-only devices used to measure the conductivity of the HTL.

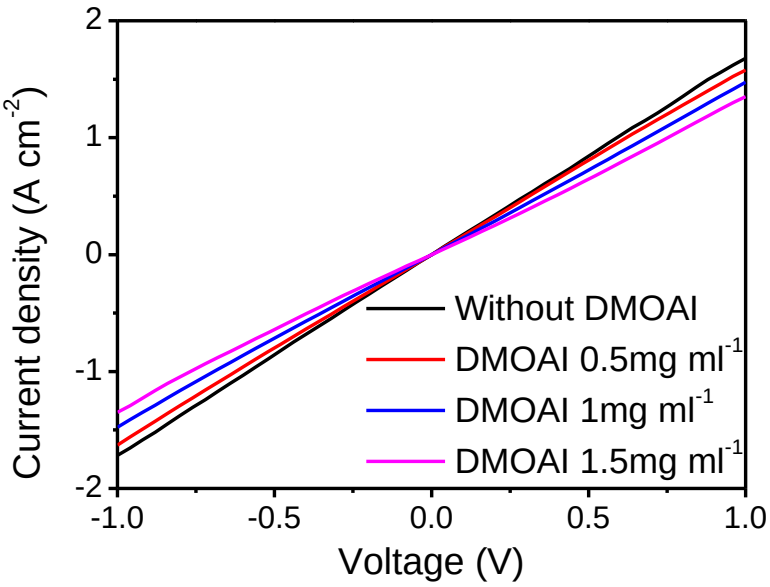

Figure S25. Vertical conductivity measurements of HTL-only devices with varying DMOAI concentrations, based on the structure shown in Figure S24.

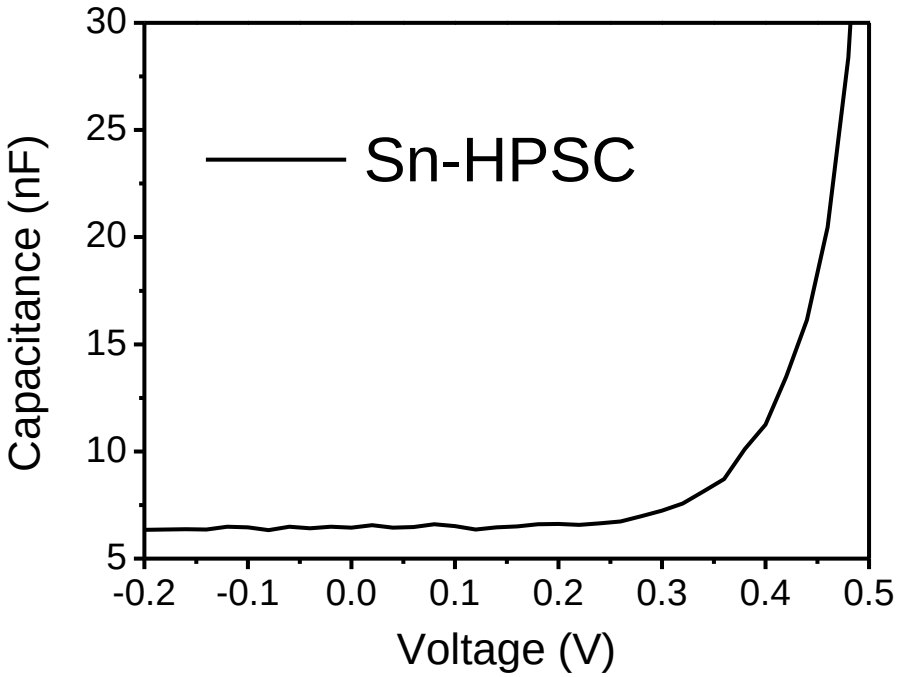

Figure S26. C-V measurement of Sn-HPSC.

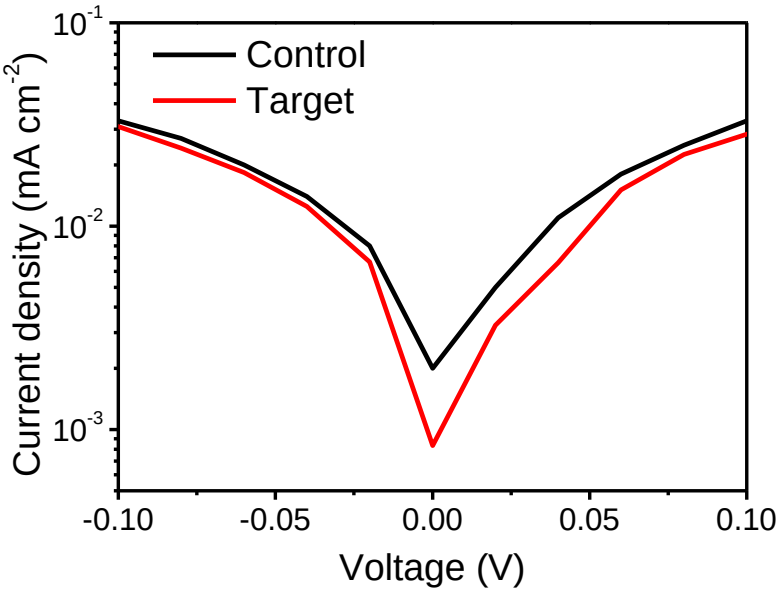

Figure S27. Enlarged dark J-V characteristic curves in region A for control and target Sn-HPSCs.

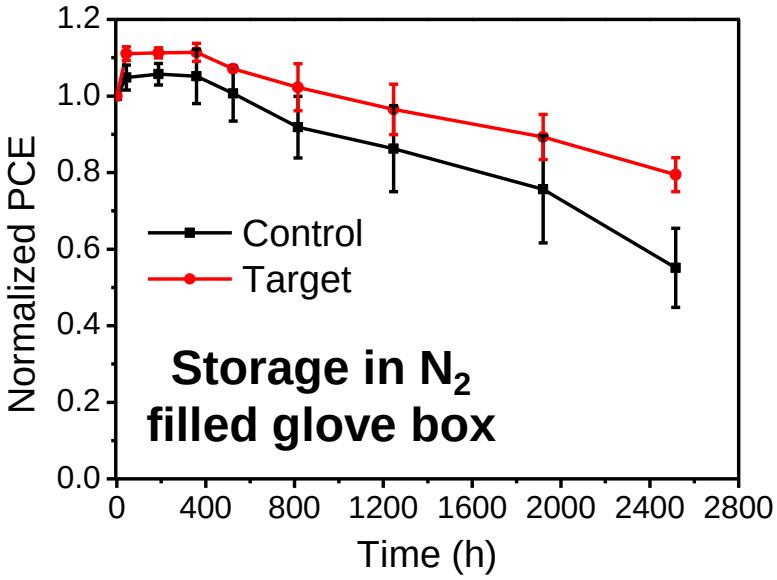

Figure S28. Normalized PCE graphs for control and target Sn-HPSCs stored under N_2 atmospheric conditions without encapsulation (measured under ambient conditions).

Table S1. Steady state photoluminescence peak position dependent on annealing time for Sn-HP growth on (a) PEDOT:PSS (control) and (b) PEDOT:PSS/DMOAI bi-layer (target) based on Figure S3.

Time (s)		0	10	20	30	60	90	120	180	600
Peak position (nm)	Control	860.5	867.5	869.5	870.5	872.0	873.0	874.0	875.5	876.0
	Target	860.0	865.0	868.0	868.5	870.5	871.5	873.0	874.5	876.0

Table S2. Key parameters obtained from Scherrer formula analysis of the (100) plane peak for control and target films, as shown in Figure S4.

Parameter	Control	Target
FWHM (°)	0.072	0.065
Peak angle (°)	14.081	14.053
Crystallite size (nm)	111.024	122.343

Table S3. Disperse ($\gamma_L{}^D$) and polar components ($\gamma_L{}^P$) of surface energy for water and diiodo-methane.

Solvents	$\boldsymbol{\gamma_L{}^D}$(mN/m)	$\boldsymbol{\gamma_L{}^P}$ (mN/m)
Water	21.8	72.8
Diiodo-methane	50.8	0

Table S4. PV parameters for Sn-HPSCs with various concentrations of DMOAI.

	V_{OC} (V)	J_{SC} (mA cm^{-2})	FF (%)	PCE (%)
Without DMOAI	0.69	22.23	67.93	10.42
DMOAI 0.5mg/ml	0.73	22.75	71.75	11.88
DMOAI 1 mg/ml	0.75	23.68	75.24	13.39
DMOAI 1.5mg/ml	0.74	22.43	70.47	11.66

Table S5. PV parameters of wide-bandgap Sn-HPSCs without and with DMOAI.

		V_{OC} (V)	J_{SC} (mA cm^{-2})	FF (%)	PCE (%)
Without DMOAI	Champion	0.76	15.13	72.69	8.35
	Average	0.74 ± 0.02	15.09 ± 0.45	70.74 ± 2.94	7.87 ± 0.44
With DMOAI	Champion	0.89	16.43	80.47	11.78
	Average	0.88 ± 0.01	16.06 ± 0.31	80.72 ± 1.35	11.37 ± 0.27